Kolmann Matthew A (Orcid ID: 0000-0001-9748-2066)

DiceCT for Fishes: Recommendations for pairing iodine contrast agents with µCT to visualize soft tissues in fishes

Matthew A. Kolmann[1,2] & Ramon S. Nagesan[3], James V. Andrews[1,4], Samuel Borstein[3], Rodrigo Tinoco Figueroa[1,4], Randal Singer[3], Matt Friedman[1,4], Hernán López-Fernández[3]

1 - University of Michigan Museum of Paleontology, University of Michigan, Ann Arbor, MI
2 – Dept. of Biology, University of Louisville, Louisville, KY
3 - Dept. of Ecology & Evolutionary Biology and Museum of Zoology, University of Michigan, Ann Arbor, MI
4 - Dept. of Earth and Environmental Sciences, University of Michigan, Ann Arbor, MI

Corresponding Author:
Matthew A. Kolmann
Department of Biology
139 Life Sciences Bldg.
University of Louisville
Louisville, Kentucky 40292
Phone: (502) 852-6771
Email: matthew.kolmann@louisville.edu

Funding Information:
Funding was provided by NSF-PRFB 1712015 to MAK, NSF-1701713 to R.N. (via D. Rabosky), NSF-PRFB 2010931 to S.B., University of Michigan Department of Earth and Environmental Sciences to R.F., Rackham Merit Fellowship (University of Michigan) to J.V.A., startup funds from the University of Michigan to M.F. and H.L.F.

Joint First Authorship:
Matthew A. Kolmann and Ramon Nagesan should be considered joint first authors and made an equal contribution to this work.

ABSTRACT

Computed tomography (CT) scanning and other high-throughput 3D visualization tools are transforming the ways we study morphology, ecology, and evolutionary biology research beyond generating vast digital repositories of anatomical data. Contrast-enhanced chemical staining methods, which render soft tissues radio-opaque when coupled with CT scanning, encompass several approaches that are growing in popularity and versatility. Of these, the various diceCT techniques that use an iodine-based solution like Lugol's have provided access to an array of morphological datasets spanning extant vertebrate lineages. This contribution outlines straightforward means for applying diceCT techniques to preserved museum specimens of cartilaginous and bony fishes, collectively representing half of vertebrate species diversity. We contrast the benefits of using either aqueous or ethylic Lugol's solutions and report few differences between these methods with respect to the time required to achieve optimal tissue contrast. We also explore differences in minimum stain duration required for different body sizes and shapes and provide recommendations for staining specimens individually or in small batches. As reported by earlier studies, we note a decrease in pH during staining with either aqueous or ethylic Lugol's. However, we could not replicate the drastic declines in pH reported elsewhere. We provide recommendations for researchers and collections staff on how to incorporate diceCT into existing curatorial practices, while offsetting risk to specimens. Finally, we outline how diceCT with Lugol's can aid ichthyologists of all kinds in visualizing anatomical structures of interest: from brains and gizzards to gas bladders and pharyngeal jaw muscles.

Keywords: bio-imaging, brain, functional morphology, muscle, soft tissues

INTRODUCTION

Bio-imaging has been central to the anatomical and histological sciences and is acquiring an ever-larger role in evolutionary biology and paleontology more recently. The benefits of techniques like x-ray computed tomographic imaging (CT) are multi-faceted. Not only can one generate CT or micro(μ)CT models which can be manipulated, dissected, or scaled *in silico*, these non-destructive radiological techniques do not harm rare or fragile specimens (Rahman et al. 2012; Manzano et al. 2015; Sutton et al. 2016; de Plessis et al. 2017; Hipsley et al. 2020; Rawson et al. 2020). Moreover, with the advent of 3D printing technologies, which pair well with surface renders from CT scans, researchers and educators alike can turn specimens into outreach tools or instructional aids. This is significant because complex structures are better understood once held in-hand (Manzano et al. 2015; Gidmark 2019; Staab, 2019; Buser et al., 2020). The contemporary imaging 'revolution' holds promise for advancing research and delivering digital phenotypic libraries of biodiversity that could compare, one day, to the flood of data obtained from next generation molecular '-omics.' (Muñoz & Price, 2019).

However, radiological techniques have only recently been modified for use in imaging fine-scale soft tissue morphologies, like nervous, gut, reproductive, and muscle tissues. Some of the most promising of these techniques fall under the category of 'contrast staining,' whereby a chemical solution like osmium tetroxide (OsO_4), Lugol's iodine (I_2KI) or phosphotungstic acid

(PTA) is gradually infused into a fixed specimen, rendering tissues increasingly radio-opaque upon uptake of the chemical stain (Metscher, 2009; Pauwels et al., 2013; Descamps et al., 2014). The popularity of iodine-based staining techniques is due to the relatively inexpensive nature and low toxicity of these compounds relative to other stains, and the ease with which these solutions can be applied to specimens (Metscher, 2009; Gignac et al., 2016; Early et al., 2020). Although staining with Lugol's solution (either in aqueous or ethylic form) is not a particularly new technique, trailblazing authors like Metscher (2009) and Gignac & Kley (2014) have made this one of the most widely used soft-tissue radiological imaging aids in the fields of evolutionary and organismal biology. One of the best contributors to the widespread use of Lugol's or 'diceCT' techniques (Gignac et al., 2016), is the straightforward, recipe-like efforts that experts have developed for their colleagues in herpetology, ornithology, and mammalogy (Hedrick et al., 2018; Watanabe et al., 2019; Callahan et al., 2021).

Callahan et al. (2021) recently published a thorough aid for those herpetologists interested in using diceCT to image snakes. Similarly, Early et al. (2020) and Hedrick et al (2018) established protocols for staining birds and bats, respectively. All these efforts build on broader, all vertebrate-level techniques explored by Gignac et al. (2016). What is lacking however, is a clear workflow for imaging fishes, the most diverse vertebrate group, and one which contains both model systems including medaka and zebrafish and extraordinary variety of sizes, shapes and tissue characteristics. Whereas some studies have used contrast staining to image one or two fish species (Brocklehurst et al., 2018), and typically model organisms (Descamps et al., 2014), few evolutionary studies have offered a workflow for those of us exploring non-model animals (but see Kolmann et al., 2018). Moreover, fishes have some of the greatest diversity of organ and sensory modalities among vertebrates, from electric organs (EOs) that some fishes use for both communication and navigation, to the photophores of midwater (mesopelagic) fishes (the most abundant vertebrates by biomass on the planet), to the muscular slings of secondary jaws located in the pharynx of fishes like morays and cichlids (Crampton et al., 2019; Martin et al., 2022; Liem & Greenwood, 1981). For example, studies have made good use of staining agents like PTA for visualizing the complex sucker disk of remoras (Echeneidae), as well as sifting and filtering epibranchial organs in carp and gobies (Cohen et al., 2018, 2020a,b; Brodnicke et al., 2022). Imaging the diversity of fishes promises to lend insights into the largest vertebrate radiation, but also serves as an anatomical atlas for animal models used for the study of human disease (Crampton et al., 2019).

We used contrast staining with Lugol's iodine alongside micro-computed tomography (μCT) scanning to visualize the soft tissue anatomy of preserved specimens across a diverse sampling of extant bony and cartilaginous fishes. This study has two primary goals. First, to provide biologists with a straightforward workflow for staining, visualizing, and de-staining preserved fish specimens. Second, to highlight the sorts of taxonomic and anatomical diversity that diceCT aids in visualizing. We address the considerations of the first goal using several objectives: (1) gauge differences in optimal staining across different sized fishes; (2) examine the effect of body shapes (compressed or cylindrical) on stain time; (3) explore the effect of 'batch' staining (staining more than one specimen in a container at a time) on stain times; and (4) contrast the efficacy of Lugol's solutions mixed in either water or 70% ethanol. Early studies have shown how Lugol's solutions can be mixed in either aqueous or ethylic solutions (Metscher, 2009); since ethylic Lugol's solution should be (near) isotonic relative to specimen

preservation fluid, we tested the utility of this technique alongside aqueous solutions (Gignac & Kley, 2014). Finally, we also address low-effort procedures for de-staining specimens in collections. We discuss how these methods can best be used by ichthyological researchers writ large, from museums and collections, to biomedical facilities, and even in the classroom.

MATERIALS & METHODS

Specimen selection and preservation:

The specimens used in this study are all accessioned at the University of Michigan Museum of Zoology (UMMZ) Fish Collection (Table 1). The specimens vary in age (collection date) from less than one year to over 95 years old. All specimens were formalin fixed and preserved in a 70% ethanol solution prior to data collection. 40 individuals (*n=40*) from 22 genera were selected from several major clades of cartilaginous and bony fishes (Table 1). The selected specimens encompass a range of body plans: laterally compressed to cylindrical, eel-like to armored, and so on. Body sizes (standard length, SL) range from 38.0-137.0 millimeters (mm) and preserved body masses ranged from 1.0-62.6 grams (g; Table 1). Figure 1 depicts our methodological workflow.

Staining protocols:

All specimens were stained in Lugol's iodine solution (Metscher, 2009; Gignac and Kley, 2014). Staining in Lugol's iodine artificially increases the density of soft tissue structures, putatively through the binding of iodine atoms with lipid cells in the preserved specimens (Gignac and Kley, 2014). This permits visualization of soft-tissue features using X-rays that would otherwise pass through them unattenuated (Metscher, 2009; Gignac and Kley, 2014) (Figure 1).

Lugol's iodine solution is most commonly a mixture of potassium iodide (KI), crystalline iodine (I_2), and deionized water: $I_2 + KI + H_2O$ (Gignac and Kley, 2014). However, we stained 36 specimens in 70% ethylic Lugol's iodine, and four specimens in a more typical aqueous Lugol's solution. Henceforth these two treatments will be referred to as "ethylic Lugol's" and "aqueous Lugol's", respectively. Both ethylic and aqueous Lugol's 1.25% solutions were prepared in 4-liter (L) containers by mixing: 100g of KI with 50g of I_2 with either 4L of 70% EtOH or 4L of deionized H_2O. Solutions were mixed using a magnetic stir rod and stirring plate until chemical components were completely dissolved (taking 24-48 hours). During mixing and for the duration of the study, containers of Lugol's solution were isolated from light, either by keeping the containers in an opaque plastic container or covered by a dark cloth. Specimens stained in aqueous Lugol's were prepared the same as described above for ethylic specimens, except for being subjected to a "step down" procedure in different ethanol concentrations (70% to 50% to 25%) prior to staining (Callahan *et al.* 2021) (Figure 1). This process lessens the potential for osmotic shock, desiccation and deformation of specimens preserved in alcohol prior to staining in aqueous solutions.

The pH of Lugol's iodine solution has been reported to decrease during the staining process, becoming more acidic as time passes (Early et al., 2020). So, we measured pH of the Lugol's solution at the beginning and end of each of the size-series samples (Table 2) with a handheld digital pH meter (PCTSTestr, Oakton, Charleston, SC, USA). However, measuring the

pH of ethylic solutions can be difficult and even commercial pH meters can be misled (Kotrba & Schilling, 2017).

To compare stain uptake rates across different body sizes and shapes, we CT imaged an abbreviated size series for six taxa (*n* =18, small, medium, large): threadfin acara *Acarichthys heckelii* (Müller & Troschel 1849), demon eartheater *Satanoperca jurupari* (Heckel 1840), and Malayan leaffish *Pristolepis fasciata* (Bleeker 1851), all of which are considered to have 'laterally compressed' body shapes. Similarly, we stained series of Two Spot Pike cichlid *Crenicichla lepidota* Heckel 1840, dwarf snakehead *Channa limbata* (Cuvier & Valenciennes 1831), and *Bivibranchia bimaculata* Vari 1985, all considered to have 'cylindrical' body shapes. (Figure 1). These 'batched' specimens (3 individuals per species) were stained as species groups in 450 ml containers of 1.25% ethylic Lugol's, with a starting pH of 6.5. DiceCT studies vary in whether they stain specimens individually or together (i.e., "batched") - in order to evaluate the effect this has on stain uptake duration, we stained additional (*n=2*) medium sized specimens of *A. heckelii* (64 mm SL) and *B. bimaculata* (69 mm SL) individually (i.e., one specimen per jar) in 450 ml of 1.25% ethylic Lugol's. These specimens were subjected to short CT scans periodically, to check on the rate of stain penetration into the body cavity (see Supplemental Table I for scanning parameters).

To test whether stain uptake rates and stain quality differed between ethylic and aqueous Lugol's solutions, we stained four (*n=4*) additional small specimens of *A. heckelii* and *B. bimaculata* (two specimens per jar) in 450 ml of 1.25% aqueous Lugol's iodine. In order to increase our taxonomic coverage, and to gauge the effectiveness of Lugol's solution for imaging particular soft-tissue anatomies of interest (e.g., electric organs, photophores, etc.), we stained another 16 specimens from different taxonomic groups (Table 1) in 200-400 ml of 1.25% ethylic Lugol's. These specimens were CT scanned after ten days, to confirm stain penetration into the body cavity (see Supplemental Table I for scanning parameters below).

Scanning protocols:

All CT data were generated using a Nikon XTH 225ST (Xtek, Tring, UK) µ-computed tomography scanner and then reconstructed using CT Pro 3D (Nikon Metrology, Tring, UK). Three-dimensional (3D) visualizations and segmentations were conducted in Dragonfly (v.2021.2, ORS, Montreal, QC), 3DSlicer (slicer.org; Fedorov et al., 2012), and Volume Graphics (v.3.3, Heidelberg, Germany). All 'quick' scans were primarily conducted at 100kV, 200uA, 250 millisecond exposure, with 1601 projections and 2 frames averaged per projection (Supplementary Table). These parameters resulted in a scan time of 13 minutes and 25 seconds, which was enough time to assess the level of staining uptake. The amperage, number of projections, and/or frame averaging were altered for collecting final, volume-render quality scans, while the length of scan depended on specimen size and stain uptake (Supplemental Table I).

The size series and ethylic Lugol's-stained specimens were scanned in intraspecific batches with three specimens (one small, one medium, and one large) packed together, then scanned and reconstructed as a single dataset. Specimens were considered fully stained when the viscera (always the last body region to become evident) were clearly visible. Similarly, the aqueous Lugol's-stained specimens were scanned two specimens at a time (single species batches). The solo stained and diversity sample specimens were all scanned individually and

using parameters that optimized image quality over scan time (Supplemental Table I). Before scanning, specimens were removed from their Lugol's bath, placed within 1.0 mm polyethylene tubing, labeled, and then heat-sealed to limit desiccation during scanning (Figure 1; Callahan et al., 2021). The specimen and its plastic housing were then placed in a styrofoam cup and stabilized with foam 'packing peanuts' to limit movement (see Callahan et al., 2021 for details of specimen stabilization for CT scanning).

Statistical Analyses:

We used the R statistical coding suite to perform all analyses (www.r-project.org). We used ANCOVA to evaluate correlations between specimen size (mass, length), specimen age, body shape (compressed *vs*. cylindrical), staining solution (ethylic or aqueous Lugol's) on stain duration and pH change. We also used ANCOVA to appraise potential differences in stain time arising from the two staining solutions. For all analyses we used the *aov* function, coupled with a Tukey Honest Significant Differences test (function *TukeyHSD*) for assessing significance. Figures plotting body size against stain duration were based on ordinary least squares (OLS) regression and differences in stain time were visualized with boxplots. We considered *p*-values at or under 0.05 as significant for all analyses.

De-staining:

Following staining and scanning (see below) all specimens were de-stained in 70% EtOH. If the specimens were part of the ethylic Lugol's staining group, then they were placed into fresh 70% EtOH. If the specimens were part of the aqueous Lugol's treatment then they were "stepped up" to 70% EtOH, spending 2-3 days each at 25%, then 50%, and finally 70% EtOH solution (Figure 1). Destaining times vary based on size of specimens and how often fresh EtOH is replaced, but can take between 3-5 weeks (Callahan et al., 2021). Destaining EtOH must be changed as the Lugol's solution leaches from the specimen into the surrounding EtOH, turning it a reddish color (for our purposes, detaining ethanol baths were only changed once). When the destaining EtOH has turned completely red, then it has reached saturation and must be changed. As the destaining continues the EtOH discolor less, and it is considered completed when the surrounding EtOH ceases changing color. All waste ethanol and Lugol's iodine was disposed of in accordance with University of Michigan Environment Health and Safety chemical waste procedures.

RESULTS

We diceCT scanned and stained a total of 40 specimens, which generated 19 quick scans and 37 high-quality scans (some individuals were scanned more than once). Optimally stained specimens, where different tissues were clearly differentiated in reconstructed slices, took over two weeks (15-18) days to fully saturate. However, we noticed that most of the soft tissues of primary interest to researchers in the past (e.g., brain, muscle) were visible and easily differentiated from the surrounding skeleton within 3-5 days of staining. Stain progression (i.e., diffusion through the specimen) is clearly visible in transverse CT slices through the specimen (Figure 2), where a "halo" of more radio-opaque tissue gradually expands deeper into the viscera. The visceral cavity and associated organs are always the last body region to stain

completely (Figure 2). We note that smaller specimens did stain slightly faster than larger specimens; however, the rate difference between larger and smaller specimens was non-significant in our analyses (length: R^2=0.007, p=0.613; mass: R^2=0.014, p=0.494) (Figure 3). We suspect that this relates to our observation that superficial tissue layers stain faster in smaller specimens, while the viscera took a similar time to stain among all specimens. We did not observe a difference in stain time among our batch- or individually- stained specimens (*p*=0.92), nor a difference among our aqueous and ethylic stained specimens (*p*=0.568) (Figure 3). We also document no difference in stain duration time for older or younger specimens (time specimens spent in collections; *p*=0.204).

We did notice a slight decrease in pH in all our Lugol's baths, from an average starting pH of 6.1 to an ending pH of 5.18. However, this decrease was not significantly different among aqueous or ethylic solutions (*p*=0.979) or different sized specimens (*p*=0.750). Finally, we found no significance between pH change, change in mass, or specimen age with specimen body shape or size (Figure 3) (Table 2).

We were able to observe a variety of soft tissues and tissues of particular interest to ichthyologists and other comparative biologists. Nervous tissue, gastrointestinal tract, connective tissue (tendon, ligament) and muscle (smooth, cardiac, and striated) were easily differentiated from surrounding tissues (Figures 4,5). We were also able to visualize the otophysic connection to the gas bladder in a soldierfish (*Myripristis*) (Figure 5B), and muscular slings in pike cichlid (*Crenicichla lepidota*) pharyngeal jaws (Figure 5C). Individual muscle fibers became apparent after 14 days in striated muscle (Figure 4). We were also clearly able to visualize reproductive structures in the climbing perch *Anabas testudineus* (Bloch 1792) (Figure 2). Gut tract, swim bladder, and the viscera in general were more apparent after 14-20 days (Figure 4); for example, the stomach and intestinal tract in taxa like boquiche *Steindachnerina bimaculata* (Steindachner 1876) (Figure 4E). Even internal parasites were obvious in some scans (*Geophagus abalios* López-Fernández & Taphorn 2004) (Figure 4D). However, we were unable to visualize with any sort of detail either the photophores in deepwater hatchet fish or the electric organs in the glass knifefish *Eigenmannia virescens* (Müller & Troschel 1849), after any duration of staining.

To assess the speed of destaining we scanned two specimens after 7 days of destaining, one that was stained in aqueous Lugol's iodine and one that was stained in 70% ethylic Lugol's iodine. In both cases, each specimen still showed a significant amount of soft tissue staining, even though qualitatively it appeared that iodine was leaching out from each specimen, as evident by a decrease in reddish external coloration. Destaining can take an extended period, and it is not known if there are ways to accelerate the process. As in Callahan et al. (2021), we assessed a specimen to be "fully" destained when there was no visible leaching of Lugol's iodine into the destaining ethanol solution.

DISCUSSION

We sought to provide insight into best practices for combining diceCT with preserved fish specimens, as well as evidence that morphologies of interest to ichthyologists can be visualized with diceCT. Overall, we see few practical differences in the implementation of either ethylic or aqueous Lugol's solutions for staining fishes. The former appears to stain tissues less

discriminately, but more rapidly (Metscher, 2009a & 2009b), while aqueous Lugol's may provide better contrast among tissue types, at least at first. Curatorial personnel might be more inclined to use the ethylic technique, given that it limits potential osmotic stress on specimens compared to an aqueous Lugol's solution. However, both methods sufficiently increase the contrast of soft tissues against the backdrop of the bony skeleton after just two weeks in solution (as in Gignac & Kley, 2014). We also found that specimens can be stained in small groups with little noticeable reduction in stain duration relative to specimens soaked individually. Our own experiences, however, lead us to recommend that when staining many specimens, it is best to do so in smaller batches of ~3-5 similarly sized individuals at a time (Kolmann et al., 2018; Figueroa et al., 2022). This is beneficial from a logistical standpoint, as many research groups do not have exclusive access to a CT scanner. Thus, having smaller and temporally staggered staining batches may help limit the disparity in stain duration among specimens while in queue for scanning (and absorbing more iodine in the interim). Finally, we found that despite differences in body size (mass, length) and body shape (cylindrical *vs*. compressed) among our specimens, that a minimum two-week bath in Lugol's solution was optimal for tissue staining in preserved fishes (Figure 3).

We did observe, albeit in only a few specimens, that extensive squamation might limit stain uptake in some fishes (e.g., lined sole *Achirus lineatus* L. 1758; see Figure 4C). This was surprising for some samples, like flatfishes, given that their compressed body shape should be more amenable to better stain uptake given their large surface area-volume ratio. However, even some of the most intensively sheathed specimens in our dataset, like armored catfishes (Loricariidae) had similar stain durations to non-armored taxa, suggesting that there is not a clear rule concerning squamation and its effect on staining time.

Researchers might also want to use diceCT for larger specimens than we used for this study; the average size fish specimen in the UMMZ collection is 50-75 mm. Several of us have found that in these cases, removing specific regions of interest from large specimens, and staining these samples rather than a whole specimen, can be helpful to reduce stain times (see Gignac & Kley, 2014). For these dissected specimens, a one- to two- week stain duration is generally more than sufficient. We also point out that slight incisions can be made into the body cavity of specimens to increase the immediate surface area available for stain uptake (essentially staining from within and without). Curators will be understandably hesitant to approve destructive practices like these; however, larger (and herbivorous) fish specimens frequently have their abdomens perforated in the field for more thorough fixation. These same incisions can reduce stain duration, as well as used for targeted injection of Lugol's into the viscera (skinning specimens can be helpful too; Gignac et al., 2016). Another option for increasing stain uptake may lie in periodically replacing old solutions with fresh Lugol's to maintain a high diffusion gradient, especially if the Lugol's solution becomes lighter in coloration during staining (Gignac & Kley, 2014; Gignac et al., 2016).

Curatorial concerns considered.

We documented a decrease in the pH of the Lugol's solution over the duration of staining. However, we could not replicate the kind of drastic decline in pH reported by Early et al. (2020), with our observed values (4-6 pH) being nowhere near the acidity (2-3 pH) required to dissolve hard tissues like bone (Nikiforuk & Sreebny, 1953; Fernández-Jalvo et al., 2014).

However, measurement of pH in ethylic solutions can be inaccurate and both our methods and previous studies may not be considering inaccuracies inherent to measuring pH in natural history collections (Kotrba & Schilling, 2017). These reports of low pH can be offset by buffering Lugol's solutions prior to staining specimens (see Dawood et al., 2020; Gray pers. comm.), but in general, these reports require greater investigation. We posit that improper storage of Lugol's solutions (i.e., exposure to light and photodecomposition of iodine), might be contributing to the declines in pH recorded by some studies. Dawood et al. (2020) suggest stabilizing staining solution pH with Sorensen's phosphate buffer as tissue shrinkage preventative, which we also recommend for fragile or rare specimens.

Although these concerns are clearly alarming for collections personnel, we would mention that the relative safety of Lugol's solution over other, harsher chemical stains (e.g., PTA, osmium tetroxide) should also be considered, as well as the reduced environmental impact of Lugol's disposal over these other methods. Finally, although some iodine will never completely leave specimens, we further document the relative ease with which Lugol's can be removed from specimens with only periodic exchange of stock ethanol needed over a few months' time.

We suggest the following for researchers interested in using museum collections for diceCT: (1) try to request specimens from large lots (i.e., only stain non-unique specimens); (2) aid curatorial staff in staining and destaining procedures to offset already high staff workloads; and (3) consider collecting your own samples, with a prior agreement in place with the collections that the deposited specimens will be used for diceCT. DiceCT can facilitate the widespread, repeatable, and readily democratic dissemination of specimen-based research. By depositing diceCT data on data repositories such as Morphosource (https://www.morphosource.org Duke University), Dryad (https://datadryad.org/stash) and Deep Blue Data (https://deepblue.lib.umich.edu/data University of Michigan), researchers can conduct collections-based research when travel or funding is limited. These repositories can track downloads, user statistics, and geographic information, allowing curatorial staff to gauge how, where, and when their collections are being used virtually. This extends the utility of a single specimen beyond that which is contained within a jar and allows collections to expand their usability to researchers who are not capable of visiting in person or to whom, for various reasons, sending loans is not possible or risky.

What can you see (and what can't you see) with diceCT?

We were successful in imaging myriad morphologies of interest to both ichthyologists and comparative anatomists with diceCT. We were able to clearly discern muscles from the surrounding skeleton in some specimens within two days of staining with aqueous Lugol's solution, like what has been documented for other vertebrates (Gignac & Kley, 2014). Other anatomical subjects of specific interest to ichthyologists, like the otophysic connection (auditory structure connecting the braincase, vertebrae, and swim bladder), pharyngeal jaw muscles, and the epibranchial organ were present after just five days (Figures 4,5). However, we did not have success in visualizing photophores or the electric organ, at least in the two taxa (deep sea hatchetfish, *Sternoptyx* sp. and the glass knifefish *Eigenmannia*, respectively) we sampled. However, one of us (M.A.K.) has seen some success in visualizing the EO in electric rays (e.g., *Narcine*) with diceCT in the past.

It is perhaps not that these tissues do not stain properly, but rather that differentiation of specialized tissue (electrocytes) from surrounding tissues is obscured even with microCT. This observation suggests that coupling diceCT methods with nanoCT or 'soft' x-ray tomography may hold promise for visualizing the more fine-scale differences in cellular and tissue structures between, for example, striated muscle and electrogenic tissues. Nano-scale CT machines, which are available as desktop units (Brunke et al., 2007), visualize structures at the sub-micron scale (0.5 µm or 500 nm) and are already available at many core facilities working on bone microstructural or even cellular differences (Peyrin et al., 2011; Zuluaga et al., 2014). These techniques are generally being used for more biomedical or model system-related research, in vertebrates like zebrafish (Ferstl et al., 2018), but nanoCT coupled with contrast-staining holds great promise for comparative anatomy (Khoury et al., 2015). It is our hope that nanoCT and contrast-staining can be used to visualize finer-scale structures like photophores and electric organs in fishes using these emerging technologies.

Summary and general recommendations

DiceCT methods are appropriate for use beyond preserved museum or biomedical specimens. When using fresh material, we and others recommend that tissue fixation (in 10% formalin, but other solutions work too) is a good first step for specimen preparation (Gignac & Kley, 2014, 2018; Decamps et al., 2014). After proper fixation is complete, staining specimens in a 1-3% aqueous or ethylic Lugol's solution for 10-14 days is sufficient to observe most soft tissues with radiological methods for specimens in the size range used in this study. Differentiation among tissues is easier to observe after 14 days in stain, and presumably iodine uptake by specimens will plateau as the diffusion gradient ablates. When using aqueous Lugol's solution, make sure to slowly transition ethanol-preserved specimens to water using a hydration series before staining (Figure 1). Likewise, consult with curatorial staff if they would prefer specimens to be soaked in buffered Lugol's solution to offset potential pH drop and soft tissue shrinkage (Dawood et al., 2020). We recommend staining several similar-sized specimens at once. This approach saves time, maximizes the lifespan of staining solutions, and minimizes chemical waste. When staining larger specimens, discuss with curatorial personnel and obtain permission to partially dissect specimens, if reducing stain time is pertinent (injection with Lugol's, in our experience, does not help penetration). Short-duration test CT scans (~30 min) provide efficient means to assess adequate stain penetration and tissue discrimination before commencing with more costly, full-length scanning. Finally, de-staining cannot remove the entirety of Lugol's solution from specimens, but soaking specimens in ethanol and periodically replacing this fluid as it becomes discolored (Callahan et al., 2021), reduces cost and time investment needed for returning specimens (close) to their original condition.

ACKNOWLEDGMENTS / FUNDING

We thank the proponents and provocateurs of diceCT and other contrast staining methods for their contributions to our fields. We thank our Reviewers for their helpful comments.

AUTHOR CONTRIBUTIONS

MK and RN, with input from RS, HLF, and MF, conceived and designed the study. RN, MK, SB, RF, JE collected the data. MK, RN, SB, RF, JE, and JVA analyzed the data. MK, RN, RS, HLF,

and MF drafted the initial version of the manuscript and all authors contributed to final versions of the manuscript.

DATA AVAILABILITY

Scan data for this project will be made available via the University of Michigan Library's Deep Blue Data repository. DOIs for each data object are provided here: https://deepblue.lib.umich.edu/data

TABLES

Table 1. Stained specimen demographics. All specimens are from University of Michigan Museum of Zoology (UMMZ).

Species	Taxonomic Authority	Family	Catalog #	# of Specimens	Standard Length (mm)	Mass (g)	Age (years)
Acarichthys heckelii	Müller & Troschel 1849	Cichlidae	216417	6	38-92	1.2-22.7	50
Satanoperca jurupari	Heckel 1840	Cichlidae	203495	3	42-95	2.2-22	87
Pristolepis fasciata	Bleeker 1851	Pristolepididae	251870	3	55-100	4.0-60.9	46
Crenicichla lepidota	Heckel 1840	Cichlidae	206086	3	40-119	1.0-21.5	43
Channa limbata	Cuvier 1831	Cichlidae	240774	3	51-137	2.1-38	25
Bivibranchia bimaculata	Vari 1985	Hemiodontidae	252549	6	40-135	0.9-43.1	3
Parapriacanthus ransonneti	von Bonde 1923	Pempheridae	183100	1	53.71	4.1	93
Anabas testudineus	Bloch 1792	Anabantidae	218102	1	108.66	45	48
Argyropelecus aculeatus	Valenciennes 1850	Sternoptychidae	227765	1	43	2.7	38
Achirus lineatus	Linnaeus 1758	Achiridae	172750	1	80	10.5	67
Ancistrus cirrhosus	Valenciennes 1836	Loricariidae	206739	1	54	3.3	43
Steindachnerina bimaculata	Steindachner 1876	Curimatidae	207781	1	95	21.7	43
Cyphocharax helleri	Steindachner 1910	Curimatidae	252559	1	63	6.7	1
Eigenmannia virescens	Valenciennes 1836	Sternopygidae	252706	1	107	2.7	1
Macrognathus semiocellatus	Roberts 1986	Mastacembelidae	243168	1	131	5	24
Myripristis kuntee	Valenciennes 1831	Holocentridae	185695	1	122	62.6	58
Noturus gyrinus	Mitchill 1817	Ictaluridae	165173	1	56	3.1	69
Parexocoetus brachypterus	Richardson 1846	Exocoetidae	250075	1	136.8	30	93
Labroides dimidiatus	Valenciennes 1839	Labridae	185602	1	66.56	4	58
Dermogenys pusilla	Kuhl & van Hasselt 1823	Zenarchopteridae	155817	1	42.28	0.5336	93
Centrogenys vaigiensis	Quoy & Gaimard 1824	Centrogenyidae	100361	1	109.59	48	90
Labrus bergylta	Bauchot & Quignard 1973	Labridae	147279	1	121.42	44	95

Table 2. pH change in Lugol's solution from beginning to end of project. All specimens are from University of Michigan Museum of Zoology (UMMZ).

Species	UMMZ Catalog #	SL (mm)	Mass (g)	Start pH	End pH	Ethylic or H_2O Solution
Acarichthys heckelii	216417	38	1.2	6.5	5.13	ethylic
Acarichthys heckelii	216417	65	7.1	6.5	5.13	ethylic
Acarichthys heckelii	216417	64	6.4	6.5	5.3	ethylic
Acarichthys heckelii	216417	92	22.7	6.5	5.13	ethylic
Acarichthys heckelii	216417	41	1.5	6.5	5.18	aqueous
Acarichthys heckelii	216417	41	1.7	6.5	5.18	aqueous
Bivibranchia bimaculata	252549	45	1.2	6.5	5.18	aqueous
Bivibranchia bimaculata	252549	42	1.1	6.5	5.18	aqueous
Bivibranchia bimaculata	252549	40	0.9	6.5	5.11	ethylic
Bivibranchia bimaculata	252549	74	5.6	6.5	5.11	ethylic
Bivibranchia bimaculata	252549	69	5.7	6.5	5.43	ethylic
Bivibranchia bimaculata	252549	135	43.1	6.5	5.11	ethylic
Channa limbata	240774	51	2.1	6.5	5.46	ethylic
Channa limbata	240774	79	7.7	6.5	5.46	ethylic
Channa limbata	240774	137	38	6.5	5.46	ethylic
Crenicichla lepidota	206086	40	1	6.5	5.13	ethylic
Crenicichla lepidota	206086	76	6.9	6.5	5.13	ethylic
Crenicichla lepidota	206086	119	21.5	6.5	5.13	ethylic
Pristolepis fasciata	251870	55	4	6.5	4.95	ethylic
Pristolepis fasciata	251870	75	19.9	6.5	4.95	ethylic
Pristolepis fasciata	251870	100	60.9	6.5	4.95	ethylic
Satanoperca jurupari	203495	42	2.2	6.5	5.19	ethylic
Satanoperca jurupari	203495	55	4.5	6.5	5.19	ethylic
Satanoperca jurupari	203495	95	22	6.5	5.19	ethylic

Supplemental Table I. Computed tomography scan parameters

FIGURE CAPTIONS

Figure 1. Sample specimen preparation and experimental design workflow for the study. All specimens were formalin-fixed and preserved in 70% ethanol prior to the study.

Figure 2. Visualization of ethylic and aqueous Lugol's stain penetration into fish (A: *Anabas testudineus*) tissues over time. (B-D): ethylic stain penetration after 24 hours, 72 hours, and 14 days. (E-G): aqueous stain penetration after 24 hours, 72 hours, and 14 days. Insets: (H)

changes in voxel range before and (I) after staining. Note the more uniform stain uptake in ethylic samples (B-D) vs. more differentiated tissues in E-G.

Figure 3. Relationship of staining times in Lugol's solution relative to body size and shape. There were no noticeable differences in stain duration between specimens soaked either in aqueous or ethylic Lugol's solutions.

Figure 4. Tomographic slices through preserved specimens showing complete stain penetration and successful 3D renderings of structures of interest to ichthyologists. (A) gill lamellae of *Satanoperca jurupari*. (B) brain render of *Noturus gyrinus*. (C) heart of *Achirus lineatus*. (D) internal parasites in *Geophagus abalios*. (E) gizzard of *Steindachnerina bimaculata.* (F) skeletal muscle fibers from the jaw adductors of *Channa limbata*. Segmentations made with 3D Slicer software suite and Volume Graphics (3.3.2).

Figure 5. 3D volume renderings of soft tissue anatomies across the diversity of living fishes. (A) segmented brain from bowfin (*Amia calva* L., UMMZ 235291), i., transverse slice through neurocranium, ii., sagittal slice through skull, iii., rendered brain ; (B) rendered otic-swim bladder connection in squirrelfish (*Myripristis kuntee*, UMMZ 185695), i., transverse slice through neurocranium, ii., sagittal slice through skull, iii., rendered swim bladder and associated skeleton; (C) segmented pharyngeal jaw and associated muscular sling from the pike cichlid (*Crenicichla lepidota*, UMMZ 206086), i., upper and lower pharyngeal jaws and associated musculature in lateral view, ii., upper and lower pharyngeal jaws and associated musculature in frontal view.

REFERENCES

Brodnicke, O.B., Hansen, C.E., Huie, J.M., Brandl, S.J. and Worsaae, K., (2022) Functional impact and trophic morphology of small, sand-sifting fishes on coral reefs. Functional Ecology.

Buser, T.J., Boyd, O.F., Cortés, Á., Donatelli, C.M., Kolmann, M.A., Luparell, J.L., Pfeiffenberger, J.A., Sidlauskas, B.L. and Summers, A.P., 2020. The natural historian's guide to the CT galaxy: step-by-step instructions for preparing and analyzing computed tomographic (CT) data using cross-platform, open access software. Integrative Organismal Biology, 2(1), p.obaa009.

Callahan, S., Crowe-Riddell, J.M., Nagesan, R.S., Gray, J.A. and Davis Rabosky, A.R., 2021. A guide for optimal iodine staining and high-throughput diceCT scanning in snakes. Ecology and evolution, 11(17), pp.11587-11603.

Cohen, K.E. and Hernandez, L.P., 2018. The complex trophic anatomy of silver carp, *Hypophthalmichthys molitrix*, highlighting a novel type of epibranchial organ. Journal of Morphology, 279(11), pp.1615-1628.

Cohen, K.E., Crawford, C.H., Hernandez, L.P., Beckert, M., Nadler, J.H. and Flammang, B.E., 2020a. Sucker with a fat lip: The soft tissues underlying the viscoelastic grip of remora adhesion. Journal of Anatomy, 237(4), pp.643-654.

Cohen, K.E., Flammang, B.E., Crawford, C.H. and Hernandez, L.P., 2020b. Knowing when to stick: touch receptors found in the remora adhesive disc. Royal Society open science, 7(1), p.190990.

Crampton, W.G., 2019. Electroreception, electrogenesis and electric signal evolution. Journal of fish biology, 95(1), pp.92-134.

Dawood, Y., Hagoort, J., Siadari, B.A., Ruijter, J.M., Gunst, Q.D., Lobe, N.H.J., Strijkers, G.J., de Bakker, B.S. and van den Hoff, M.J.B., 2021. Reducing soft-tissue shrinkage artefacts caused by staining with Lugol's solution. Scientific reports, 11(1), pp.1-12.

Descamps, E., Sochacka, A., De Kegel, B., Van Loo, D., Van Hoorebeke, L. and Adriaens, D., 2014. Soft tissue discrimination with contrast agents using micro-CT scanning. Belgian Journal of Zoology, 144(1).

du Plessis, A., Broeckhoven, C., Guelpa, A., le Roux, S.G.., 2017. Laboratory x-ray micro-computed tomography: a user guideline for biological samples. Gigascience. 6(6):1-11. PMID: 28419369.

Early, C.M., Morhardt, A.C., Cleland, T.P., Milensky, C.M., Kavich, G.M. and James, H.F., 2020. Chemical effects of diceCT staining protocols on fluid-preserved avian specimens. PloS one, 15(9), p.e0238783.

Fedorov A., Beichel R., Kalpathy-Cramer J., Finet J., Fillion-Robin J-C., Pujol S., Bauer C., Jennings D., Fennessy F.M., Sonka M., Buatti J., Aylward S.R., Miller J.V., Pieper S., Kikinis R. 2012. 3D Slicer as an Image Computing Platform for the Quantitative Imaging Network. Magnetic Resonance Imaging. 30(9):1323-41. PMID: 22770690.

Fernández-Jalvo, Y., Andrews, P., Sevilla, P. and Requejo, V., 2014. Digestion versus abrasion features in rodent bones. Lethaia, 47(3), pp.323-336.

Ferstl, S., Metscher, B., Müller, M., Allner, S., Dierolf, M., Busse, M., Achterhold, K., Gleich, B. and Pfeiffer, F., 2018. Laboratory-based X-ray NanoCT Explores Morphology of a Zebrafish Embryo. Microscopy and Microanalysis, 24(S2), pp.184-185.

Figueroa, R.T., Goodvin, D., Kolmann, M.A., Coates, M.I., Caron, A.M., Friedman, M. and Giles, S., 2022. Exceptional fossil preservation and evolution of the ray-finned fish brain. bioRxiv.

Gidmark, N.J., 2019, June. Build your body (no, seriously, actually make it): integrating 2D-and 3D-maker-culture into a comparative vertebrate anatomy course. In Journal of Morphology (Vol. 280, pp. S35-S35). 111 RIVER ST, HOBOKEN 07030-5774, NJ USA: WILEY.

Gignac, P.M. and Kley, N.J., 2014. Iodine-enhanced micro- CT imaging: Methodological refinements for the study of the soft-tissue anatomy of post- embryon ic vertebrates. Journal of Experimental Zoology Part B: Molecular and Developmental Evolution, 322(3), pp.166-176.

Gignac, P.M., Kley, N.J., Clarke, J.A., Colbert, M.W., Morhardt, A.C., Cerio, D., Cost, I.N., Cox, P.G., Daza, J.D., Early, C.M., Echols, M.S., Henkelman, R.M., Herdina, A.N., Holliday, C.M., Li, Z., Mahlow, K., Merchant, S., Müller, J., Orsbon, C.P., Paluh, D.J., Thies, M.L., Tsai, H.P. and Witmer, L.M. (2016), Diffusible iodine-based contrast-enhanced computed tomography (diceCT): an emerging tool for rapid, high-resolution, 3-D imaging of metazoan soft tissues. J. Anat., 228: 889-909. https://doi.org/10.1111/joa.12449

Gignac, P.M. and Kley, N.J., 2018. The utility of diceCT imaging for high-throughput comparative neuroanatomical studies. Brain, Behavior and Evolution, 91, pp.180-190.

Hedrick, B.P., Yohe, L., Vander Linden, A., Dávalos, L.M., Sears, K., Sadier, A., Rossiter, S.J., Davies, K.T. and Dumont, E., 2018. Assessing soft-tissue shrinkage estimates in museum specimens imaged with diffusible iodine-based contrast-enhanced computed tomography (diceCT). Microscopy and Microanalysis, 24(3), pp.284-291.

Hipsley, C.A., Aguilar, R., Black, J.R., & Hocknull, S.A. 2020. High-throughput microCT scanning of small specimens: preparation, packing, parameters and post-processing. Sci Rep 10, 13863.

Khoury, B.M., Bigelow, E.M., Smith, L.M., Schlecht, S.H., Scheller, E.L., Andarawis-Puri, N. and Jepsen, K.J., 2015. The use of nano-computed tomography to enhance musculoskeletal research. Connective Tissue Research, 56(2), pp.106-119.

Kolmann, M.A., Huie, J.M., Evans, K. and Summers, A.P., 2018. Specialized specialists and the narrow niche fallacy: a tale of scale-feeding fishes. Royal Society open science, 5(1), p.171581.

Kotrba, M. and Schilling, L.H., 2017. Measurement of pH in ethanol, distilled water, and their mixtures: on the assessment of pH in ethanol-based natural history wet collections and the detrimental aspects of dilution with distilled water. In Collection Forum (Vol. 31, No. 1-2, pp. 84-101). Soc. for the Pres. of Natural History Collections.

Lanzetti, A. and Ekdale, E.G., 2021. Enhancing CT imaging: A safe protocol to stain and de-stain rare fetal museum specimens using diffusible iodine-based staining (diceCT). Journal of Anatomy.

Liem, K.F. and Greenwood, P.H., 1981. A functional approach to the phylogeny of the pharyngognath teleosts. American zoologist, 21(1), pp.83-101.

Manzano, B.L., Means, B.K., Begley, C.T. and Zechini, M., 2015. Using digital 3D scanning to create “artifictions” of the passenger pigeon and harelip sucker, two extinct species in eastern North America: the future examines the past. Ethnobiology Letters, 6(2), pp.232-241.

Martin, R.P., Davis, M.P. and Smith, W.L., 2022. The impact of evolutionary trade-offs among bioluminescent organs and body shape in the deep sea: A case study on lanternfishes. Deep Sea Research Part I: Oceanographic Research Papers, 184, p.103769.

Metscher, B.D., 2009a. MicroCT for comparative morphology: simple staining methods allow high-contrast 3D imaging of diverse non-mineralized animal tissues. BMC physiology, 9(1), pp.1-14.

Metscher, B.D., 2009b. Micro-CT for developmental biology: a versatile tool for high-contrast 3-D imaging at histological resolutions. Dev Dyn 238, pp. 632–640.

Muñoz, M.M. and Price, S.A., 2019. The future is bright for evolutionary morphology and biomechanics in the era of big data. Integrative and comparative biology, 59(3), pp.599-603.

Pauwels, E., Van Loo, D., Cornillie, P., Brabant, L. and Van Hoorebeke, L., 2013. An exploratory study of contrast agents for soft tissue visualization by means of high resolution X-ray computed tomography imaging. Journal of microscopy, 250(1), pp.21 -31.

Peyrin, F., Pacureanu, A. and Langer, M., 2011, September. 3D microscopic imaging by synchrotron radiation micro/nano-CT. In 2011 18th IEEE International Conference on Image Processing (pp. 3057-3060). IEEE.

Rahman, I.A., Adcock, K. and Garwood, R.J., 2012. Virtual fossils: a new resource for science communication in paleontology. Evolution: Education and Outreach, 5(4), pp.635-641.

Rawson, S.D., Maksimcuka, J., Withers, P.J., & Cartmell, S.H. 2020. X-ray computed tomography in life sciences. BMC Biol 18, 21. DOI: 10.1186/s12915-020-0753-2

Rutledge, K.M., Summers, A.P. and Kolmann, M.A., 2019. Killing them softly: Ontogeny of jaw mechanics and stiffness in mollusk-feeding freshwater stingrays. Journal of morphology, 280(6), pp.796-808.

Schulz-Mirbach, T., Metscher, B. and Ladich, F., 2012. Relationship between swim bladder morphology and hearing abilities–a case study on Asian and African cichlids.

Schulz-Mirbach, T., Heß, M., Metscher, B.D. and Ladich, F., 2013. A unique swim bladder-inner ear connection in a teleost fish revealed by a combined high-resolution microtomographic and three-dimensional histological study. BMC biology, 11(1), pp.1-13.

Staab, K.L., 2019, June. Specimen preparation projects and visual study guides exhibited as art: engaging undergraduates and the general public in vertebrate morphology. In Journal of Morphology (Vol. 280, pp. S36-S37). 111 RIVER ST, HOBOKEN 07030-5774, NJ USA: WILEY.

Sutton, M., Rahman, I., & Garwood, R. 2016. Virtual Paleontology - An Overview. The Paleontological Society Papers, 22, 1-20. doi:10.1017/scs.2017.5

Watanabe, A., Gignac, P.M., Balanoff, A.M., Green, T.L., Kley, N.J. and Norell, M.A., 2019. Are endocasts good proxies for brain size and shape in archosaurs throughout ontogeny?. Journal of Anatomy, 234(3), pp.291-305.

Zuluaga, M.A., Orkisz, M., Dong, P., Pacureanu, A., Gouttenoire, P.J. and Peyrin, F., 2014. Bone canalicular network segmentation in 3D nano-CT images through geodesic voting and image tessellation. Physics in Medicine & Biology, 59(9), p.2155.

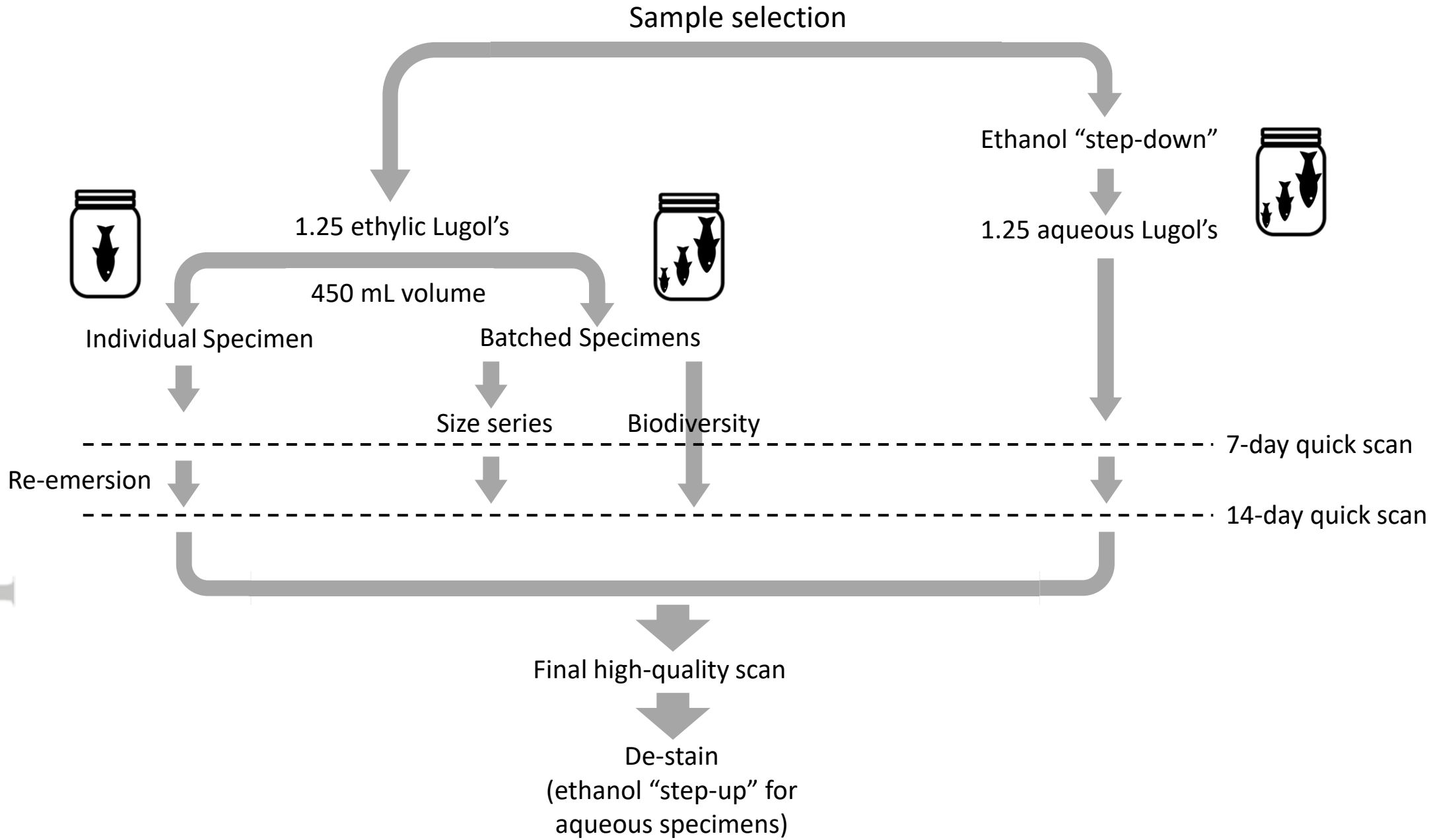

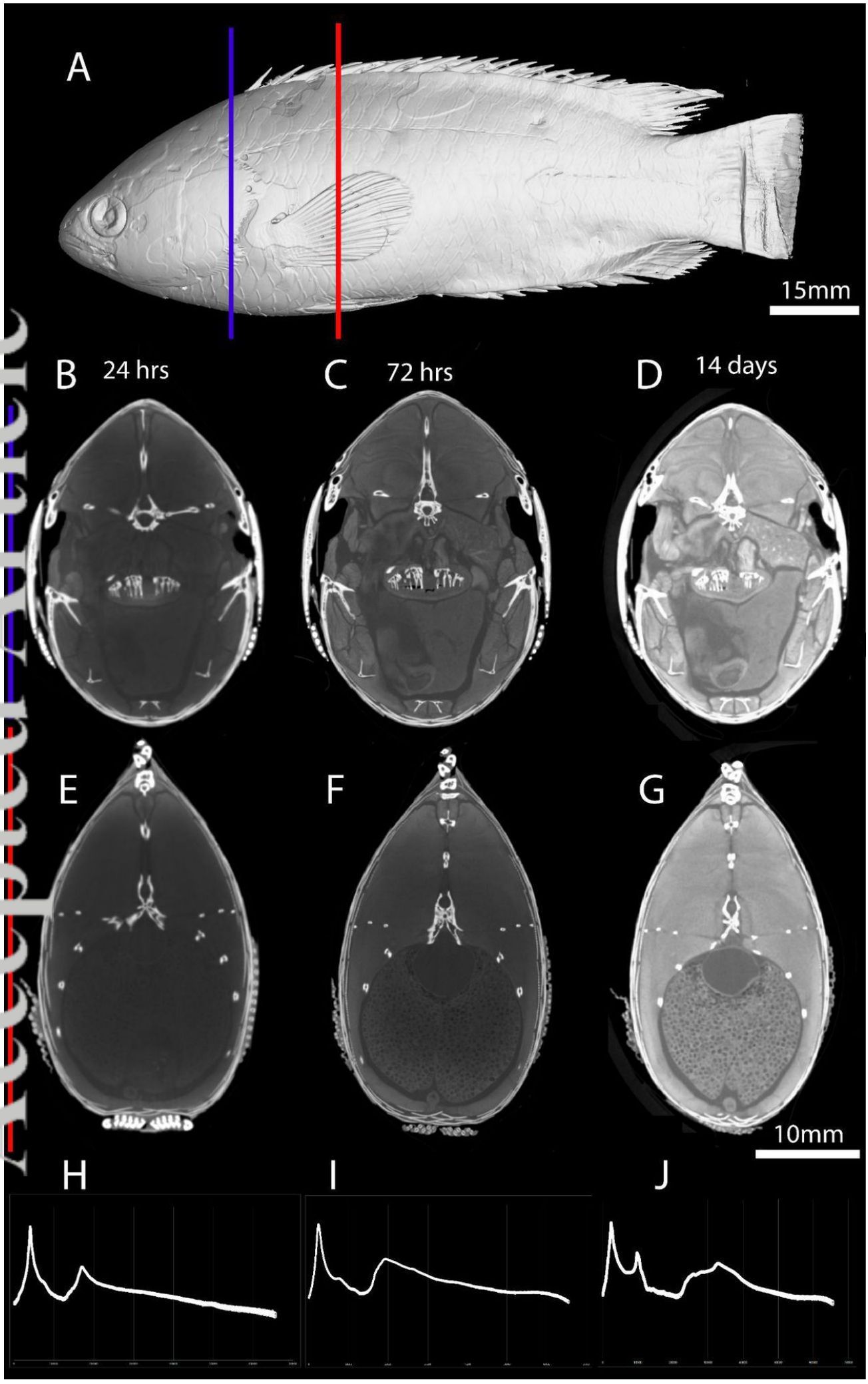

Figure 2 - Anabas stain time visual tracker.jpg

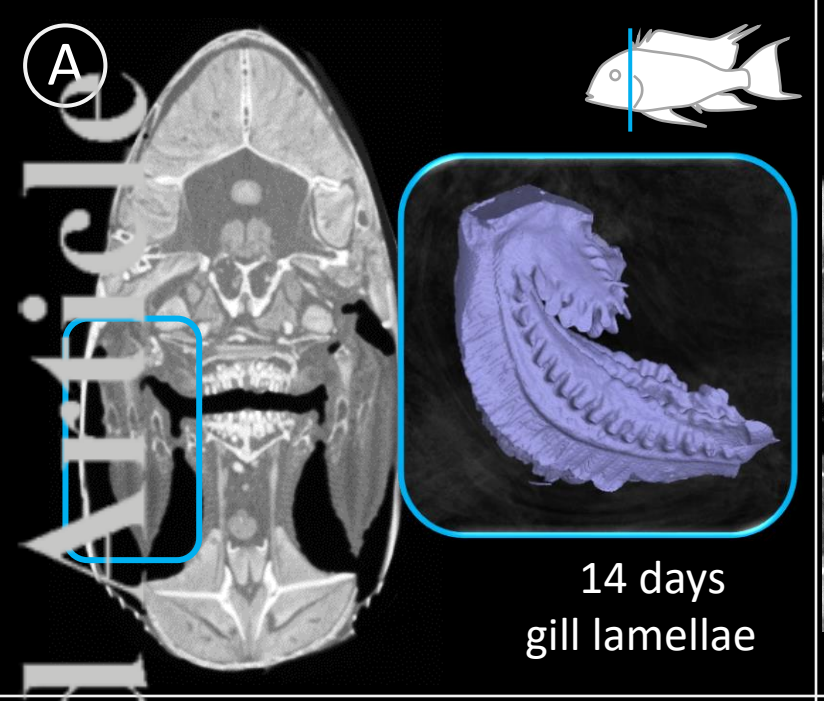

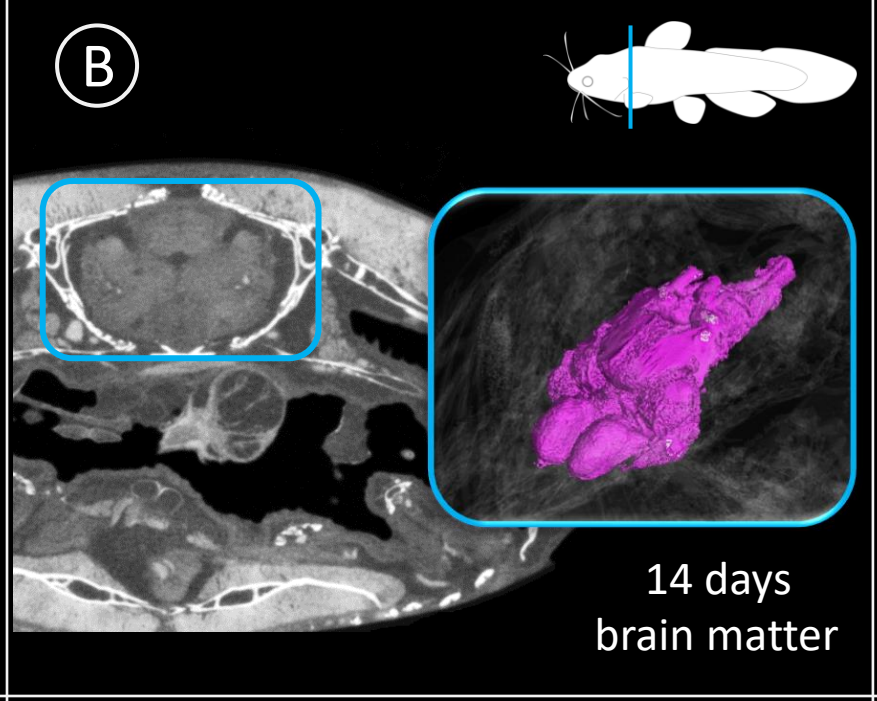

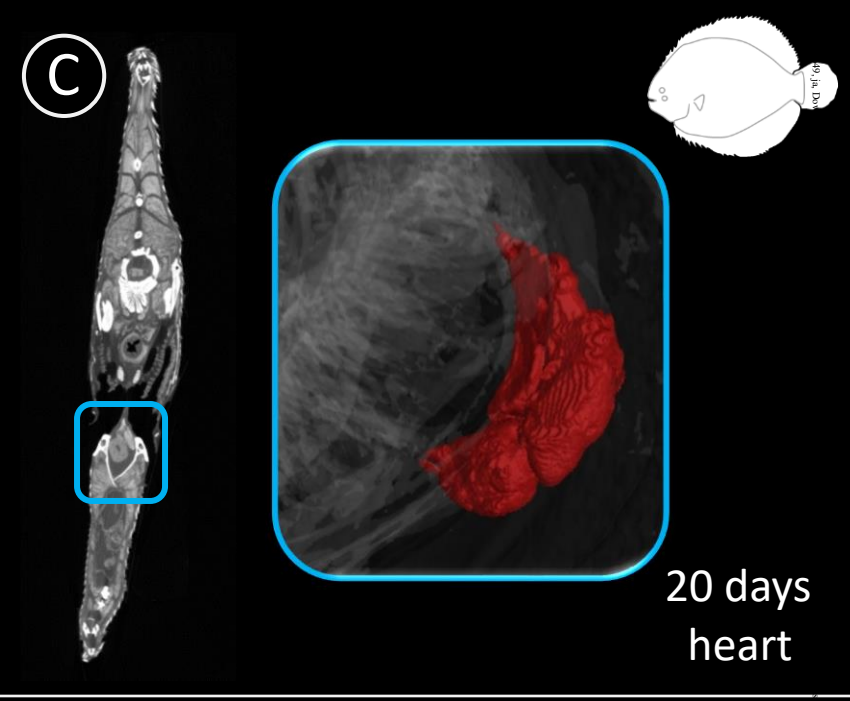

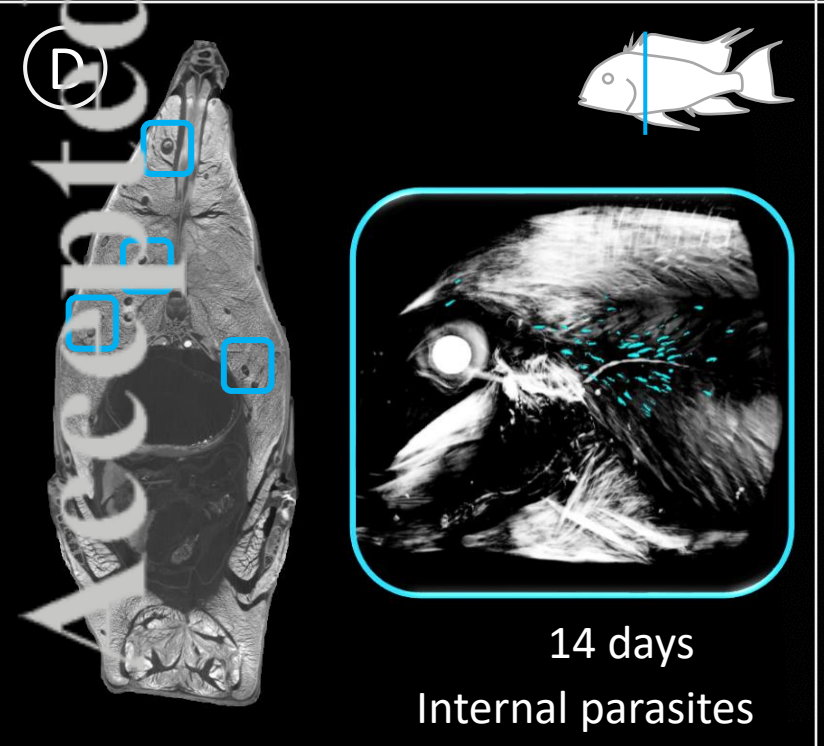

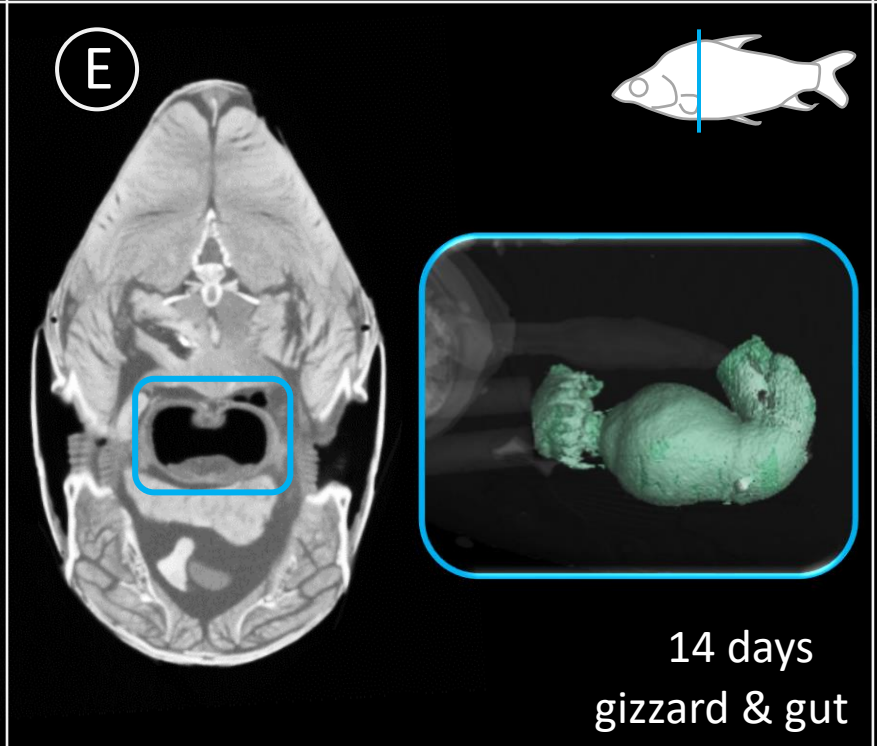

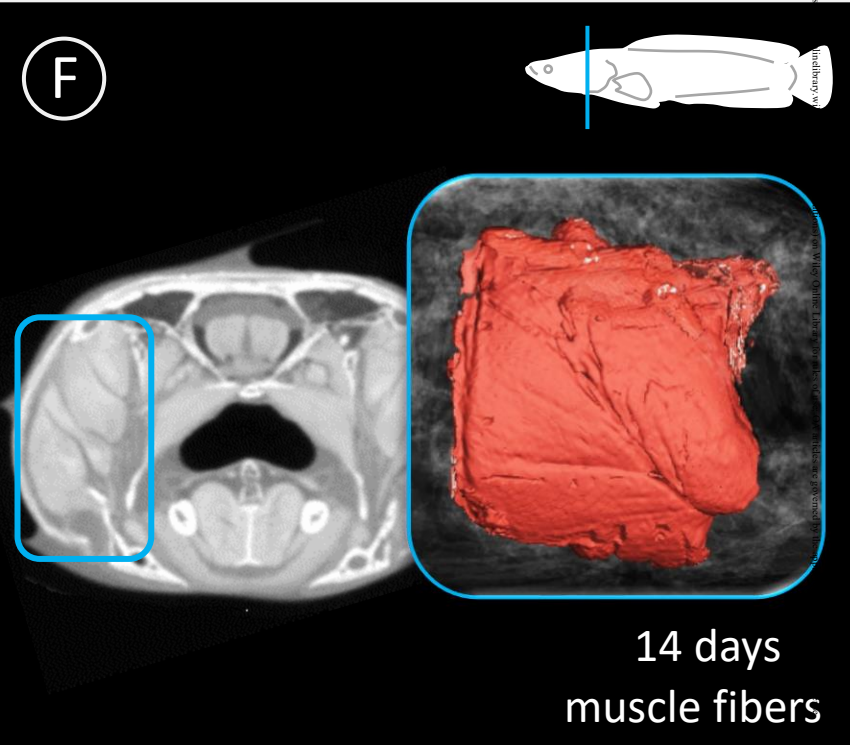

(A)

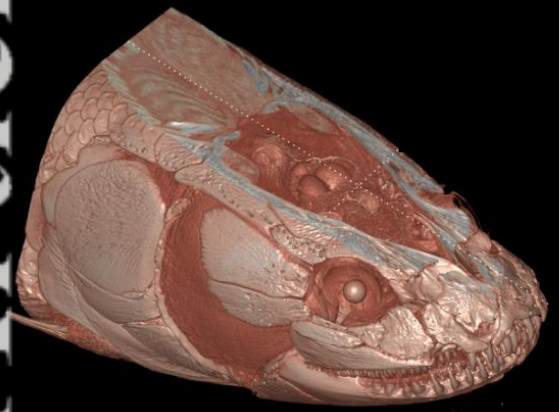

i.

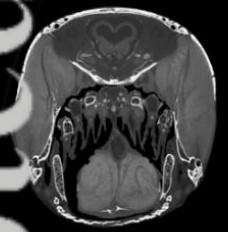

ii.

iii.

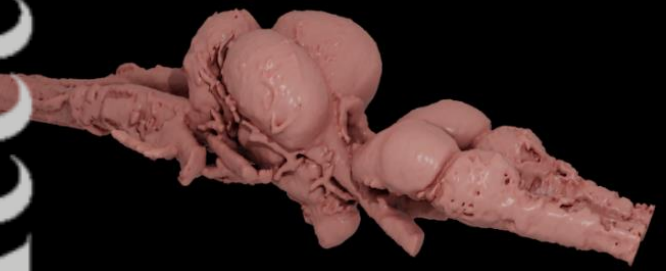

(B)

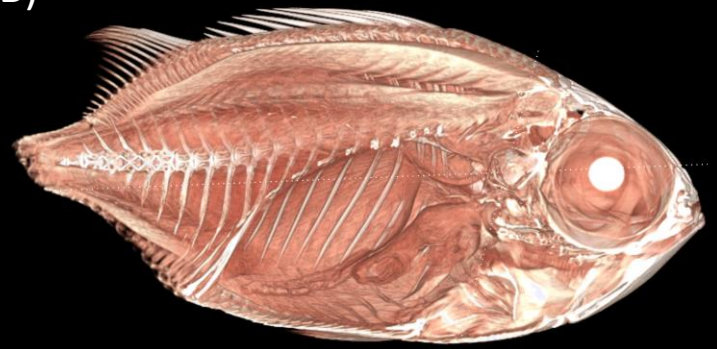

i.

ii.

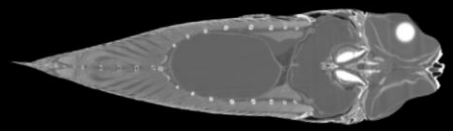

iii.

(C)

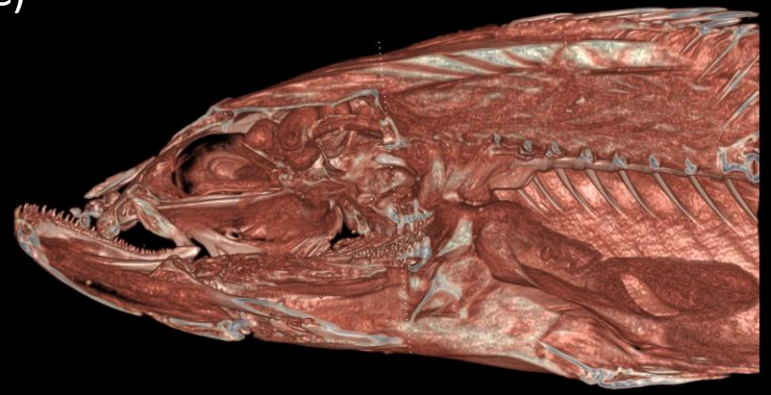

i.

ii.

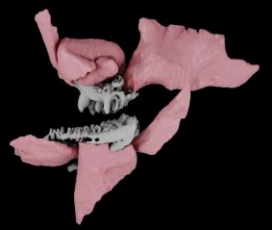

iii.

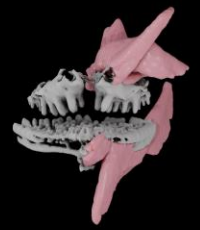

Significance statement:

Our paper, "DiceCT for Fishes: Recommendations for pairing iodine contrast agents with μCT to visualize soft tissues in fishes" adapts a popular method for visualizing soft tissues in vertebrates and evaluates the techniques effectiveness in the largest vertebrate radiation, ray-finned fishes. Here, we evaluate effectiveness of different Lugol's staining solutions and outline a general procedure for how researchers can use these techniques to visualize tissues like muscle, brain matter, and gastrointestinal tract in museum specimens. We discuss means to make the staining process more efficient and address curatorial concerns about specimen damage – making recommendations for using museums specimens in as low-impact a way as possible. We think this will be of importance to the broad readership of Journal of Fish Biology – of interest to researchers interested in anatomy, physiology, and applied biology of fishes.

Sincerely,

The authors as represented by Dr. Matt Kolmann

Note -I was unable to find documentation on the preferred format of these significance statements on the JFB website, so please forgive any deviations from expectations.